TAO, Vol. 7, No. 4, 467-487 , December 1996

Crustal Structure of the Northeastern Taiwan Area From Seismic Refraction Data and Its Tectonic Implications

Win-Bin Cheng [1,2] , Chengsung Wang[3] and Chuen-Tien Shyu[2]

(Manuscript received 20 July 1996, in final form 23 November 1996)

ABSTRACT

Seismic refraction data from onshore and offshore experiments in the eastern-northeastern Taiwan region were used to study the velocity structure by the two-dimensional ray-tracing method. In the velocity model, a structural fault boundary located beneath the Longitudinal Valley was used to separate the northern Coastal Range (CR) on the eastern side from the eastern flank of the Central Range (EFCR) on the western side. The P-wave velocities from the surface to the depth of 12-15 km varied from 3.9 to 5.8 km/s beneath the CR and from 4.8 to 6.1 km/s beneath the EFCR. Comparing the velocity structures along various latitudes, it was found that the CR extends northward to 24.2°N. The velocity structures of the CR, the Hsinchen Ridge (HR) and the Yaeyama Ridge (YR) indicate that the HR and the YR both belong to the same type of tectonic unit as the CR. To the north of 24.2°N, the velocity structure of the Ilan Ridge (IR), located between the EFCR and the southwestern end of the Ryukyu arc, is similar to that of the EFCR; hence, probably indicating it is the northeastern extension of the EFCR. This suggests that the EFCR bends eastward and belongs to the same tectonic unit as the southwestern Ryukyu arc. From a comparison of the velocity structures of the CR, EFCR and of other typical continental arcs, orogens and oceanic arcs in the literature, it can be concluded that the northern CR belongs to an oceanic arc and that the EFCR is a continental arc. Further more, from the analysis of the velocity structures beneath the CR and EFCR, it is believed that the upper crust of the CR is weaker in strength than the EFCR, which means that the arc-continent collision is not an appropriate model for the formation of Taiwan island.

(Key words: Seismic refraction, Ray-tracing, P-wave velocity structure, Coastal Range, Eastern flank of the Central Range, Arc-arc collision)

[1] Seismological Observation Center, Central Weather Bureau, 64 Kung-Yuan Road, Taipei, Taiwan, R.O.C.

[2] Institute of Oceanography, National Taiwan University, P.O. Box 23-13, Taipei, Taiwan, R.O.C.

[3] Institute of Applied Geophysics, National Taiwan Ocean University, Keelung, Taiwan, R.O.C.

1. INTRODUCTION

Located at the junction of the Eurasian plate, Philippine Sea plate and South China Sea (Figure 1), the Taiwan region is one example of an active collision tectonics. From numerous geophysical and geological studies of this region (e.g., Biq, 1965; Bowin *et al.*, 1978; Tsai *et al.*, 1981; Letouzey and Kimura, 1986; Pelletier and Stephan, 1986; Yu *et al.*, 1990), the collision suture between the Eurasian and the Philippine Sea plates is generally believed to be the Longitudinal Valley (LV) (Figures 1 and 2), which separates the Coastal Range (CR) in the east from the rest of Taiwan island. To the east of the LV is the narrow CR, made up of Miocene to Pliocene andesitic volcanic bodies and younger agglomerate and turbidite deposits (e.g., Ho, 1986; Lundberg and Dorsey, 1988). To the west of the LV is the main body of Taiwan, composed of a pre-Tertiary metamorphic basement overlain by Paleogene low-grade metamorphosed sediments, Neogene folded and thrusted sedimentary rock layers and Quaternary alluvial deposits (e.g., Ho, 1986). The Tananao Schist (TS) (Figure 2), proposed by Yen (1954), is a pre-Tertiary metamorphic complex and forms the oldest geologic tectonic element of Taiwan which constituting the eastern flank of the Central Range (EFCR) geologic province.

Some geophysical studies have shown that there are actually distinct differences in the crust structure between the CR and the EFCR. The seismic experiment by Tsai *et al.* (1974) and the earthquake travel time analysis by Lee *et al.* (1986) provided some information as to the crustal velocity structure of the CR and EFCR. From the gravity, magnetic, seismic and geologic data of eastern Taiwan and its offshore areas, Hu and Chen (1986) showed that a tectonic break separates the CR from the EFCR. However, the nature of the northward extension of the CR and EFCR has not been understood. To the west and south of the Nanao Basin (NB), there exists a ENE ($N70^{o}$) and then SE ($N130^{o}$) trending ridge that includes the Hsinchen Ridge (HR) and the Yaeyama Ridge (YR) (Figure 1). Although the topography shows that the CR , HR and YR are in fact a continuous ridges (Figure 1), whether or not they belong to the same geological unit is an issue which still needs further study.

In this study, with the use of seismic refraction data from three seismic experiments conducted separately in 1985, 1993 and 1995 and the two-dimensional ray-tracing method, the velocity profiles in the eastern Taiwan area were constructed and then used to investigate the northward and eastward extensions of the CR and the EFCR. The relationship between the CR, the HR and the YR and between the EFCR and Ryukyu arc (RA) in terms of the velocity structures in the profiles are also discussed.

2. SEISMIC DATA USED

In this paper, for the construction of the velocity model, three sets of seismic data from controlled sources in experiments conducted separately in July 1985, September 1993 and August 1995 were used. The location of the profiles are shown in Figure 2.

The 1985 data set was obtained in an experiment of a Sino-American cooperative study (e.g., Hagen *et al.*, 1988) which deployed ocean bottom seismometers (OBSs) to the east of Taiwan island. Profiles L85-1 and L85-2 (Figure 2) were taken from Hagen *et al.* (1988). Profile L85-1 was used to discuss the velocity structure of the YR while profile L85-2 was

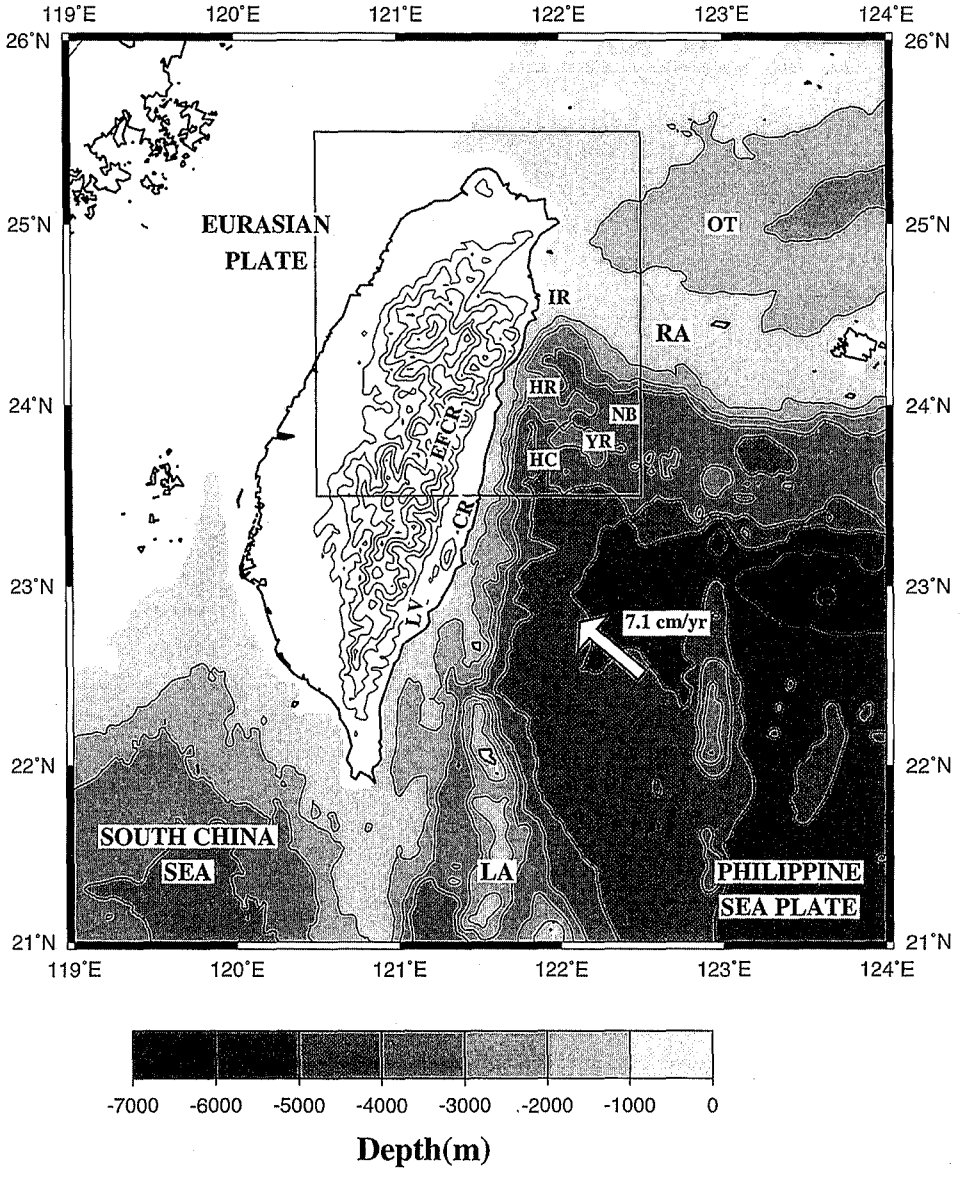

Fig. 1. Study area of this paper (blocked portion), with the plate tectonic setting and topography in the Taiwan region as the background. The Coastal Range (CR) decreases its elevation rapidly to sea level near 24°N and then links to the ENE (N70°) and the SE (N130°) trending ridge that includes the Hsinchen Ridge (HR) and the Yaeyama Ridge (YR). EFCR represents the eastern flank of the Central Range; LV, the Longitudinal Valley; NB, the Nanao Basin; RA, the Ryukyu arc; LA, the Luzon arc; OT, the Okinawa Trough; IR, the Ilan Ridge; and HC, represents the Hualien canyon.

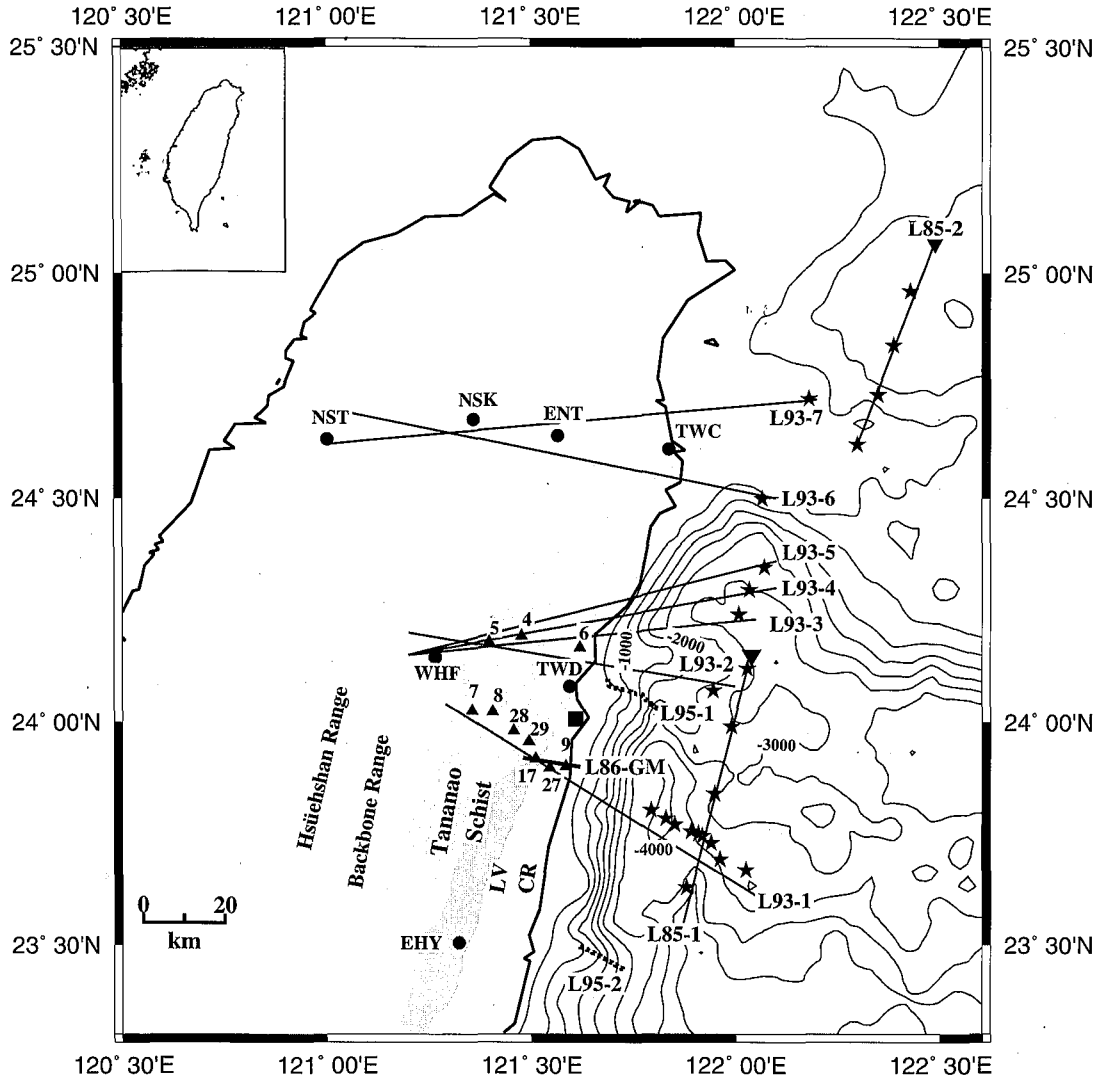

Fig. 2. Locations (solid lines) of the velocity profiles constructed in this study. Two broken solid lines indicate the locations of shot lines of the R/V Maurice Ewing in 1995. The heavy solid line south of Hualien city (solid square) indicates the location of the gravity and magnetic profiles taken from Hu and Chen (1986). CR represents the Coastal Range; LV is the Longitudinal Valley. The bathymetric contour interval is 500 meters. The solid triangles on the land side are the PANDA-2 stations. Solid circles are the CWBSN stations. Solid stars are the explosion sources. The inverted triangles on lines L85-1 and L85-2 are the OBS-C and OBS-TS shown in Figures 9 and 10.

used for that of the Ilan Ridge (IR; Yu and Hong, 1992; Song, 1994) and the Okinawa Trough (OT) and to compare them with the velocity structure beneath the EFCR and the RA (Figure 1).

The 1993 experiment was carried out in the Hualien area (e.g., Wang *et al.*, 1995). In the sea, the controlled sources were detonated at approximately 150 m in depth. Seismic signals were recorded by the Central Weather Bureau Seismographic Network (CWBSN) and a portable telemetric seismic array (PANDA-2) developed by Memphis State University (Chiu *et al.*, 1991) and deployed by the Institute of Earth Sciences, Academia Sinica in Taipei, Taiwan. The construction of the velocity structures beneath the CR and the EFCR along L93-1 was based on the seismic records of 8 explosion shots obtained by land stations (Figure 2). The velocity structures along L93-2 to L93-5 were based on seismograms of the explosions recorded by three PANDA-2 stations and the CWBSN station WHF (Figure 2). In a similar way, the velocity structures along L93-6 and L93-7 were based on seismograms of explosive sources recorded by four CWBSN stations, namely TWC, ENT, NSK and NST (Figure 2). All of these velocity profiles were used to discuss the latitudinal variations of the velocity structure beneath the CR and the EFCR.

In August and September of 1995, a comprehensive deep seismic imaging program (the TAICRUST program) was carried out in the offshore areas of Taiwan (Liu, 1995). Profiles L95-1 and L95-2 (Figure 2) made use of the TWD and EHY stations of the CWBSN and the controlled sources released from a 20-airgun array towed by the R/V Maurice Ewing of Columbia University of the U.S.A. These two profiles were used to construct the detailed velocity structure of the CR at 23.5°N and 24°N.

3. DATA ANALYSIS AND INTERPRETATION

In this study, it is assumed that the velocity in each layer increases with a certain gradient, and a two-dimensional forward modeling technique based on the asymptotic ray theory (Cerveny *et al.*, 1977) was used to obtain the travel time for a given model. The adoption of the velocity gradient model is believed to better represent the actual velocity-depth profile than the alternative homogeneous layer models (e.g. Kennett, 1977; Whitmarsh, 1978). The program RAYAMP-PC (Clossley, 1987) was adopted for interactive computing. This program allowed for the rapid testing of two-dimensional, laterally heterogeneous velocity models for travel time consistency with the data. For different source-receiver distances, the travel time curves of the first arrivals of seismic waves emitted by the explosions and air-gun sources corresponded to different ray paths in the velocity model. In order to make it better understood how the ray-tracing method was used to construct the velocity model, the ray paths of the first arrivals are briefly described here. Later arrivals need not be described, however, because the ray-tracing technique is similar. The first arrivals can be the refracted phases from the crust (referred to as the Pr phase), the reflected phases from interfaces in the crust (referred to as the PiP phase) or from the Moho discontinuity (referred to as the PmP phase). In Figure 3, the Pr phase is designated as r1, r2, ..., and the PiP phase as i1, i2, ..., depending on the deepest layer they reached. Profile L93-1 (Figure 3) is taken as an example. The record sections for shots S1, S4, S7 and S8 are shown in Figure 4. A remarkable phase i2, appearing at offsets of 30-50 km in Figure 4a, is interpreted as representative of the reflected waves from the bottom

of the 5.2-5.8 km/s layer in Figure 3b. The upper crust of the CR is characterized by a delayed arrival branch r1 which can be explained as the refracted arrivals from the 3.9-4.5 km/s layer in Figure 3b.

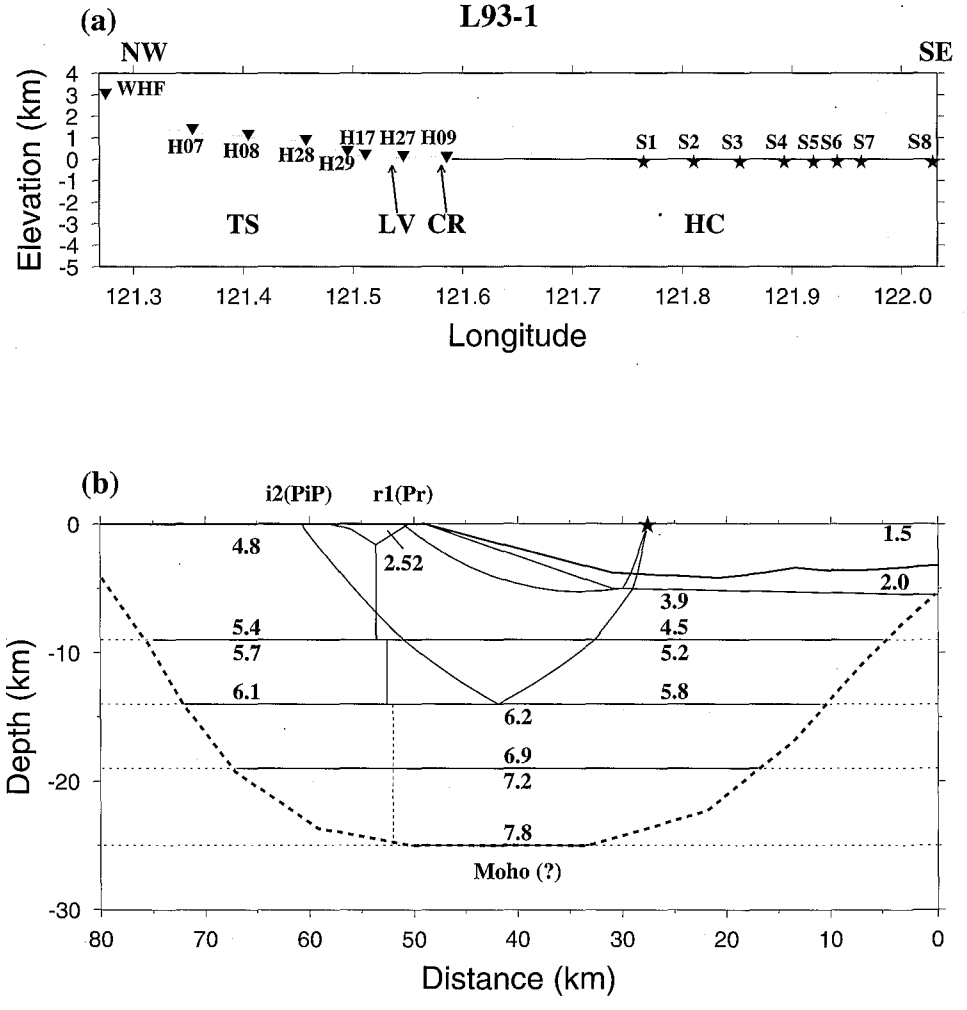

Fig. 3. (a) Topographic and (b) P-wave velocity structures of profile L93-1. The ray paths of the reflected (PiP phase) and refracted (Pr phase) waves used in this study are also shown. The velocities at the top and bottom of each layer are presented in kilometers per second. The major feature of the model is a prominent discontinuity, the Longitudinal Valley Fault, in the upper crust within the Longitudinal Valley (LV). Areas of good velocity control for the upper to lower crust (inside the dashed heavy line) were derived from the examination of the ray-tracings for each shot point and are indicated. TS is the Tananao Schist; CR is the Coastal Range; and HC is the Hualien Canyon. Vertical exaggeration is taken as 2.6:1 for (a) and 1.2:1 for (b).

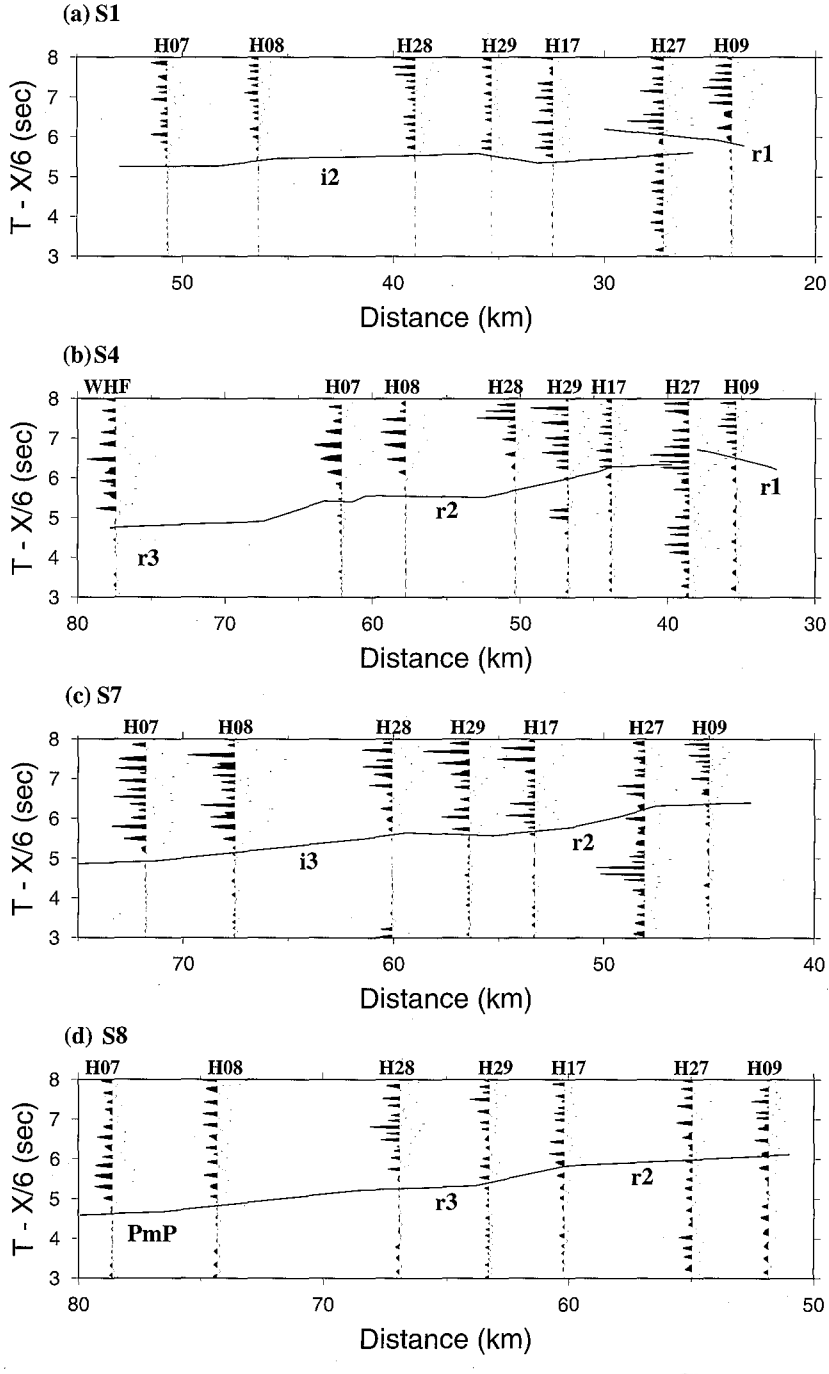

Fig. 4. Observed seismograms and predicted travel time curves of shot points (a) S1, (b) S4, (c) S7 and (d) S8 along profile L93-1. Observed seismograms were digitally band-pass filtered (2-8 Hz) to suppress ground noise. The travel time curves calculated from the model are superimposed on the observed record section. See text for explanation.

The seismic velocity models presented in this paper represent the simplest structures that best fit the travel times of phases identified in the shot records. In most cases, the calculated travel times agree with the data to within 0.1 s. Nowhere, in fact, do they diverge by more than 0.3 s. Before modeling, a static correction (with velocity 4.0 km/s) was applied to each seismogram for receiver elevation. These corrections appeared to be adequate, as indicated by the generally good agreement between the calculated first arrival times and the observed data. In modeling, 1.5 km/s was taken to be the velocity of the water layer and the source was located at the same depth beneath sea level. The amplitudes of the seismograms shown in this study (except for the record sections for L95-1 and L95-2) were normalized individually to the maximum amplitude in the first 10 seconds of the record, so they could not be strictly compared between traces.

3.1 Profile L86-GM

In order to recognize the existence and location of the vertical boundary (LV fault) described here earlier, the gravity and magnetic sections L86-GM were used (Figure 2) along with the analytical signal analysis technique of Hsu *et al.* (1996).

Figures 5a and 5b show the gravity and magnetic profiles along line L86-GM in Figure 2. Figures 5c and 5d show the amplitude curves of the analytic signal (Hsu *et al.*, 1996) for the gravity and magnetic profiles, respectively. The boundary beneath the LV was determined (b1 in Figure 5e) by picking the maximum amplitude in Figures 5c and 5d. This boundary was used in the following analysis of the velocity models.

3.2 Profile L93-1

As shown in Figure 3b, the velocity model for profile L93-1 is represented by a two-dimensional seismic velocity model that is composed of two discrete and independently derived "blocks" which are connected by a near vertical boundary, the LV boundary. The depth of the base of the sedimentary layer (2.0 km/s layer) under the shot points is at the depth of about 5.5 km. It decreases in depth and thickness from shot point S1 to station H09. The thickness of the sedimentary layer is about 2 km beneath point S8 and tapers northwestward toward the station H09. Beneath the onland 2.52 km/s sedimentary wedge (Chen and Wang, 1994) in the LV, the 3.9-4.5 km/s and 5.2-5.8 km/s layers are separated from the 4.8-5.4 km/s and 5.7-6.1 layers by a vertical boundary (Figure 3b). These layers are underlain by two planner layers with velocities of 6.2-6.9 km/s and 7.2-7.8 km/s.

In Figures 4a-4d, the travel time curves predicted by the model are superimposed on the observed vertical-component record sections. The arrival phase r1 at the stations H09 and H27 (located on the CR and LV, respectively) is delayed about 0.3 to 0.5 s compared to the i2 phase observed at other stations located on the EFCR in the S1 and S4 sections (Figures 4a and 4b). In the S7 and S8 sections (Figures 4c and 4d), this delay is not clear since the increasing offset makes the rays penetrate to deeper layers in Figure 3b. The waveforms also reflect the larger background noise which appeared at H09 and H27 compared to that at the other stations. This can be due to the site effect. For the shot point S7 (Figure 4c), high energy is recognized in an offset range of 45-57 km (denoted by r2) and 60-73 km (denoted by i3). These phases are

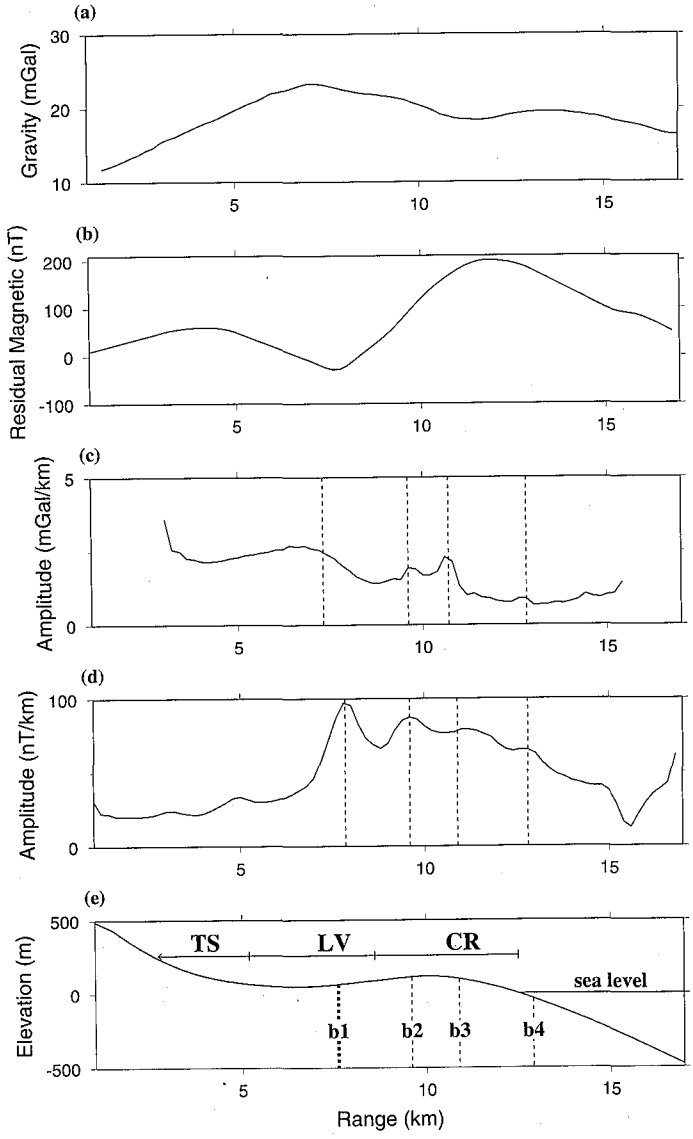

Fig. 5. Geological boundaries determined from gravity and magnetic data using the analytical signal method developed by Hsu et al. (1996). (a) Observed Bouguer gravity. (b) Observed residual magnetic. (c) Gravity amplitude calculated from (a) with the dotted vertical lines showing the probable locations of the geological boundaries. (d) Same as (c) but calculated from magnetic data. (e) Overlap of the topographic and calculated geological boundaries with the heavy dotted vertical line b1 showing the locations of the main geological boundaries between the EFCR and CR. Vertical exaggeration is taken as 5.0:1 for (e). TS represents the Tananao Schist; LV is the Longitudinal Valley; and CR is the Coastal Range.

interpreted as having refracted from the 5.2-5.8 km/s layer and reflected from the bottom of the 6.2-6.9 km/s layer, respectively. However, for the shot point S8 (Figure 4d), clear arrivals are observed at offsets greater than 70 km, which are interpreted as the PmP (Moho reflection). Thus, the Moho depth could be about 25 km beneath profile L93-1, but this is another issue which still requires further investigation.

3.3 Profile L93-2

The apparent velocity of the first arrival phase of profile L93-2 (Figure 6a top) is about 6.0 km/s. These arrivals is delayed about 0.5 to 1 second, compared with those in the record section on profile L93-1 (Figure 4). In terms of its major features, the model for L93-2 is similar to that for L93-1, although it does contain a thinner sedimentary layer and thicker 3.9-4.5 km/s layer and 5.2-5.8 km/s layers (Figure 6a bottom half). The total thickness of the 3.9-4.5 km/s layer ranges from about 7 km under the shot point to about 9 km under the coastline, whereas the thickness of the 5.2-5.8 km/s layer is poorly constrained owing to the limitation of the limited length of the profile.

3.4 Profile L93-3, L93-4 and L93-5

The velocity models for profiles L93-3, L93-4 and L93-5 (Figures 6b-6d bottom halves) are similar to those models described previously, but the thickness of the 3.9-4.5 km/s layer progressively decreases from L93-3 to L93-5, ranging from about 5 km at L93-3 to about 2 km at L93-5. In contrast, the thickness of the 5.2-5.8 km/s layer increases progressively from about 6 km to 12 km for L93-3 and L93-5, respectively.

3.5 Profile L93-6

The model for profile L93-6 (Figure 6e) is characterized by a very thin, almost invisible, sedimentary layer and a high velocity sublayer under the shot point. The difference between the velocity structures of L93-6 and L93-5 (Figures 6d and 6e bottom halves) is obvious, though the distance between the shot points for these two profiles is only 20 km apart. The thickness of the 5.3-5.85 km/s layer is 3.5 km under the shot point but 5 km near the vertical boundary. A sublayer with a velocity of 6.0 km/s is required to have reflection i2 (Figure 6e bottom half) at an offset of around 60 km. The i3 phase can be interpreted as a reflection from the bottom of the midcrust layer with velocity 6.2-6.8 km/s.

3.6 Profile L93-7

Comparing the record section of L93-7 (Figure 6f) with that of L93-6 (Figure 6e), it is clear that the travel time curves of the first arrivals are smooth. These smooth curves can be easily interpreted as refracted phases from a three-layer model as shown in Figure 6f.

3.7 Profile L95-1

The velocity model for profile L95-1 (Figure 7b) is similar to the eastern part of profile L93-1 (Figure 3b). Profile L95-1 contains a shallow ocean floor downdip to the east, a

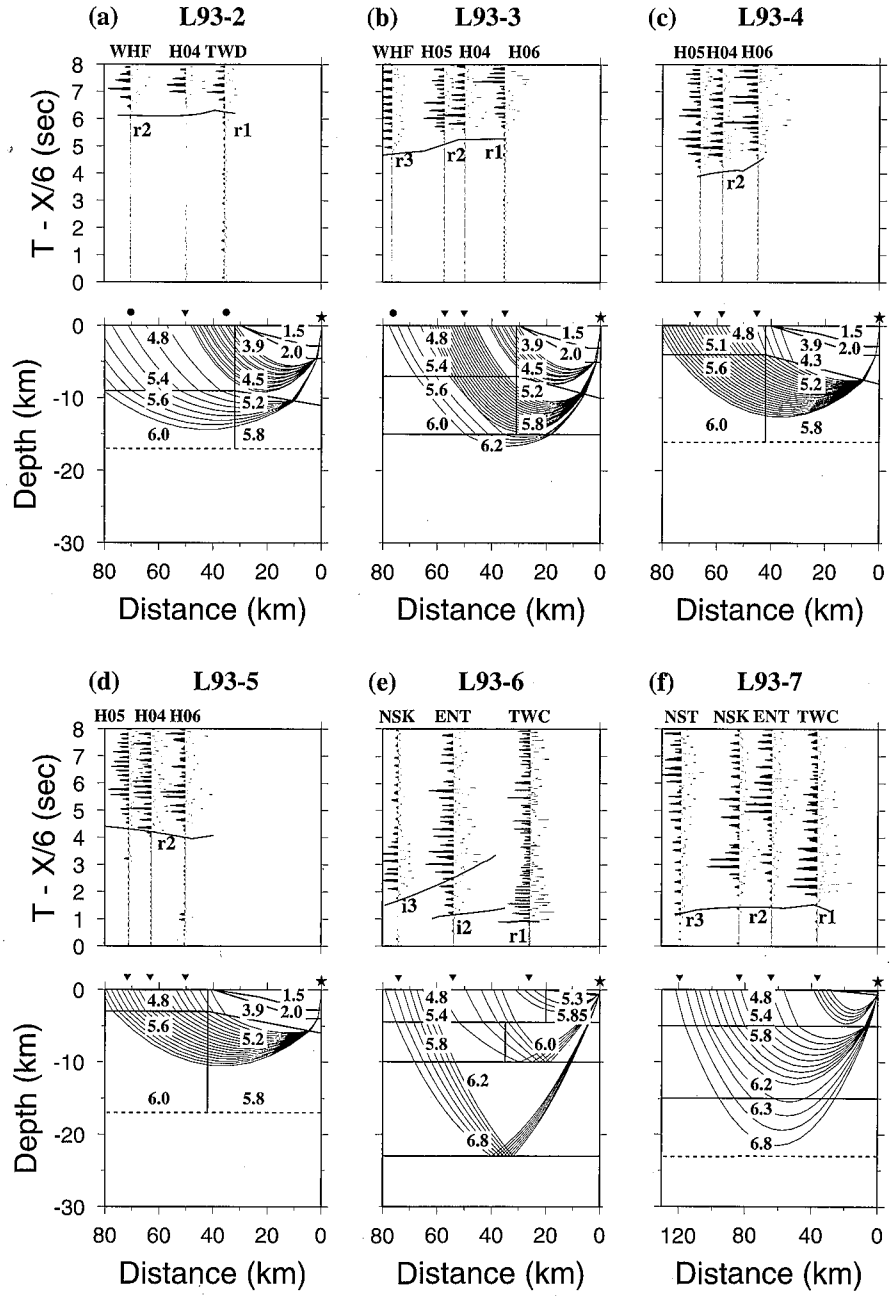

Fig. 6. Observed seismograms (top portions) and predicted travel time (bottom halves) along profile L93-2 (a) to L93-7 (f). Numbers shown in the lower halves of the diagrams are velocities in kilometers per second. The PiP and Pr phases, appearing in the top diagrams are the same as in Figure 3. Vertical exaggeration is taken as 1.9:1 for bottom halves of (a) to (e), and as 3.1:1 for the same in (f).

3.9-4.5 km/s layer and a 5.2-5.8 km/s layer. The thickness of the former ranges from 4.5 km under the shot points to 5 km beneath station TWD, while the latter, similar to that described in the model for L93-1 (Figure 3b), is about 5 km in the center of the shot points but diminishes to about 3.5 km under station TWD. The i1 and i2 phases are interpreted here as wide-angle reflections from the top and the bottom of this layer, respectively. A series of strongest later arrivals MT appear at 9.5-15 km offset (Figure 7a), and they are interpreted as multiples (see also Cheng and Wang, 1995), which means that their ray paths include one or more reflections between the free surface and the ocean floor.

3.8 Profile L95-2

The velocity model of profile L95-2 is shown in Figure 8b. Its eastern part of is similar to that of L93-1 (Figure 3b). Profile L95-2 contains a 3.9-4.4 km/s layer and a 5.1-5.7 km/s layer. However, in the western part of the model, the 3.9-4.4 km/s layer comes in contact with a 2.5-2.9 km/s sedimentary layer and the 5.1-5.7 km/s layer with a 4.8-5.3 km/s layer. The amplitude of the i2 phase is stronger than the r2 phase at the 31-35 km offset (Figure 8a), but these two phases cannot be separated at an offset greater than 38 km. The travel times of these two phases were calculated using the reflected and refracted paths in the model (Figure 8b).

3.9 Profile L85-1

The model for L85-1 is characterized by an area of downwarping and crustal thickening structures (Figure 9b). The dramatic feature of this model is in the thickness of its low-velocity sedimentary layer which ranges from about 3 km just south of the OBS-C (0 km offset) to about 4-5 km halfway between the OBS-C and the southernmost shot (60 km offset) where it then progressively decreases to about 1.5 km underneath. The sediment structure was mainly determined from the first arrivals observed at an offset less than 10-20 km (Figure 9a, i1). The thickness and depth of the 3.9-4.5, 5.2-5.8 and 6.2-6.8 km/s layers under the sedimentary layer beneath the three shot points (offset 35-60 km) are mainly similar to those in the eastern part of L93-1 (Figure 3b).

3.10 Profile L85-2

The model for L85-2 (Figure 10b) is similar to that of profile L93-7 (Figure 6f). Characterized by a thin sedimentary layer and high velocity sublayers under the shot points, it has a 4.8 km/s layer thickness of about 3.5 km, and a 5.4-6.0 km/s layer thickness of about 11 km.

4. TECTONIC INTERPRETATIONS

In this study, the model represents the simplest structure to fit the data whereas the true structure of the region is probably somewhat more complicated. There are few well-defined later phases, meaning that the model is primarily based on the travel times of the first arrivals. The wide spacing of both the shots and stations does not allow that the detailed surface geology be taken into account in the fitting of travel times. Nevertheless, the models reveal the main features of the velocity structure in the northeastern Taiwan area.

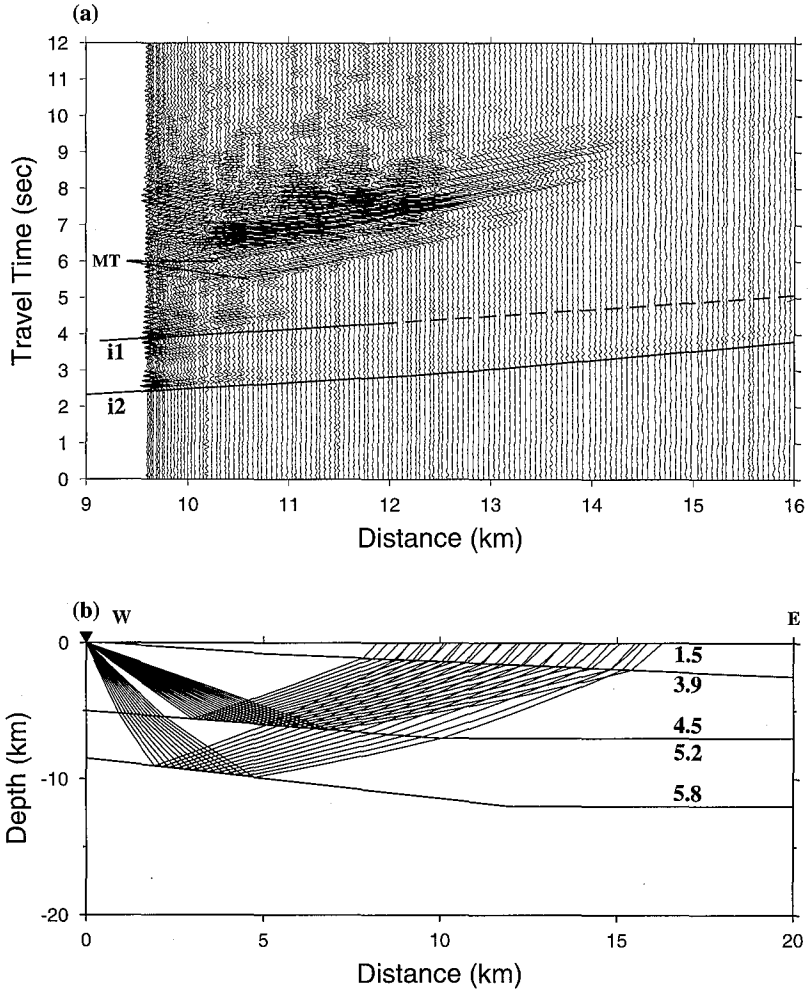

Fig. 7. (a) Observed seismograms recorded by the TWD station and calculated travel time curves along profile L95-1. Strong wavetrains appearing at offset distances of 10-15 km are interpreted as multiples (MT). (b) Ray diagram and velocity structure. Vertical exaggeration is taken as 2.6:1 for (b).

Figure 11 shows the velocity models constructed in this study together with the average crustal structure of the continental arcs and the orogens (Christensen and Mooney, 1995) and typical oceanic arc (e.g. the Kyushu-Palau Ridge) (Ludwig *et al.*, 1973). For the convenience of comparison between the velocity columns, all the sedimentary layers were removed in each velocity column in Figure 11 (where there was a sedimentary layer in the original velocity column, the base of the sedimentary layer was taken as zero depth). Based on the results of this study, to the west of the LV fault (Figure 11a), all models have a common basement (4.8-5.4 km/s layer) and a subbasement (5.6-6.4 km/s layer). The thickness of the basement is about 9 km near L93-1 (24°N), but decreases to about 3 km near L93-5 (Tailuko) and then increases to

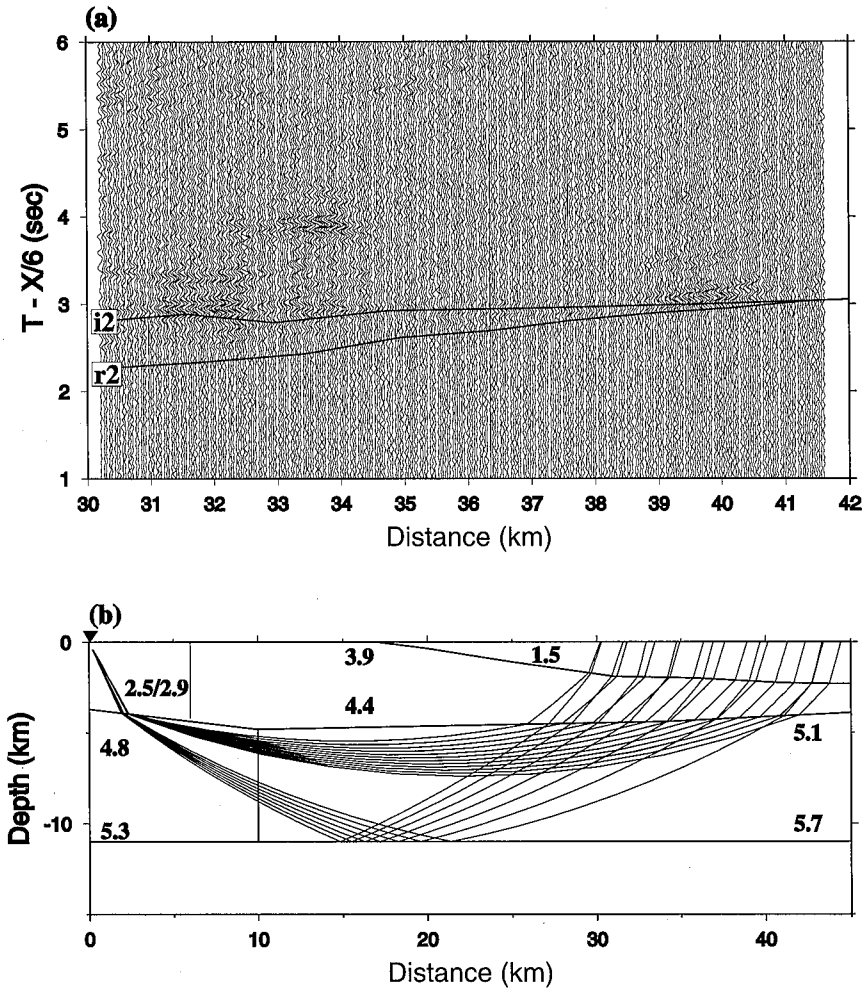

Fig. 8. (a) Observed seismograms recorded by the EHY station and calculated travel time curves along profile L95-2. The i2 and r2 phases are explained as reflected and refracted waves. (b) Velocity structure and ray diagram, with the vertical exaggeration taken as 1:1.

about 5 km at L93-7 (Ilan Plain) and to about 4 km at L85-2 (Ilan Ridge). In contrast, the thickness of the subbasement progressively increases northwards and then thins near the Ilan Plain and Ilan Ridge. The eight models on the right in Figure 11a can be divided into two groups, such that Group A represents the variation in the velocity structure beneath the Tananao Schist (the EFCR), while Group B represents the crust of the southern and southwestern end of the Ryukyu arc. The similarity in the velocity structures shown in Figure 11a suggests that the EFCR bends eastward near 24.5°N and should belong to the same tectonic unit as the southwestern Ryukyu arc (Figure 12). This eastward bending feature has also been revealed in seismic tomographic studies (e.g., Chen, 1995; Ma, *et al.*, 1996) and in the geological study of pre-Miocene (Kizaki, 1986).

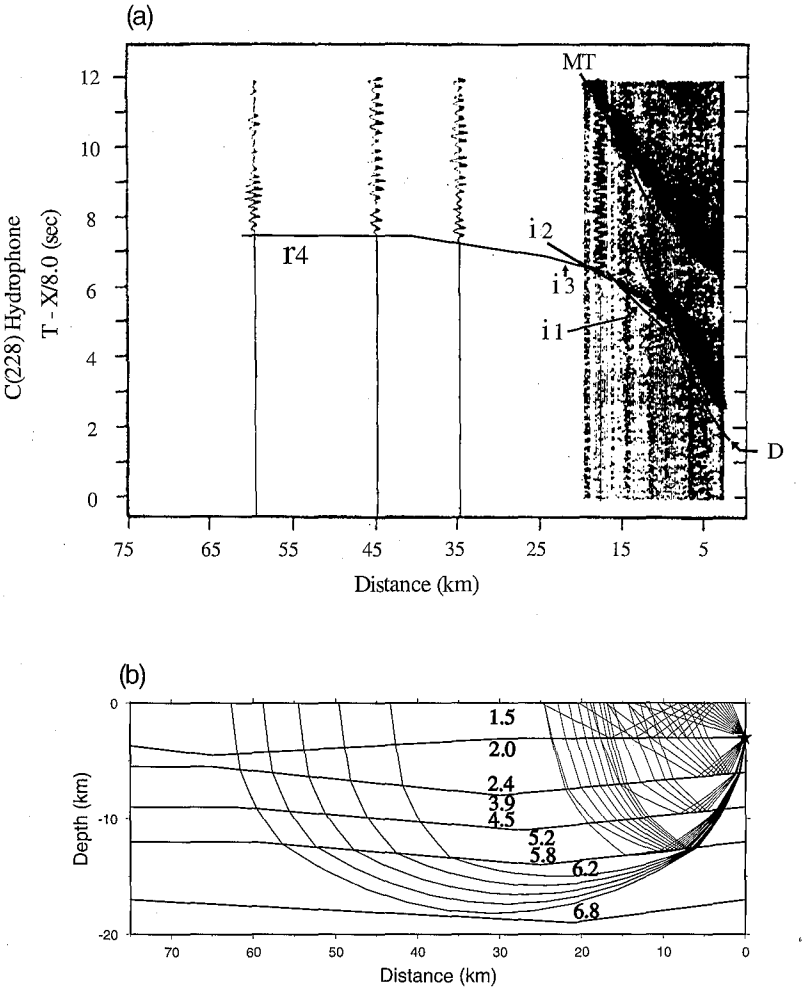

Fig. 9. (a) Observed seismograms recorded by the OBS-C and predicted travel time curves along profile L85-1. The D and MT phases are explained as directed waves and multiples, respectively. (b) Velocity structure and ray diagram, with the vertical exaggeration taken as 1.4:1.

To the east of the LV fault (Figure 11b), the thickness of the 3.9-4.5 km/s layer increases from about 3.5 km at L93-1 (northern part of the CR) to about 7 km at L93-2 (the HR) and then decreases to about 2 km at L93-5 (westernmost end of the NB). The variation in the thickness of the 5.2-5.8 km/s layer shows a similar trend to that of the 3.9-4.5 km/s layer to the south of L93-2 (the HR). However, unlike the variability of the trend of the 3.9-4.5 km/s layer, the thickness of this layer progressively increases northward from L93-2 and the layer itself ends near L93-5 (the northwesternmost part of the NB). This implies that the velocity structure of the CR extends northwards to about 24.2°N. Profile L93-2 obviously has a thicker 3.9-4.5 km/s layer than its northern and southern adjacent places (L95-1 and L93-3), reflecting the uplifted bathymetry around the Hsinchen Ridge and the low velocity materials contained be-

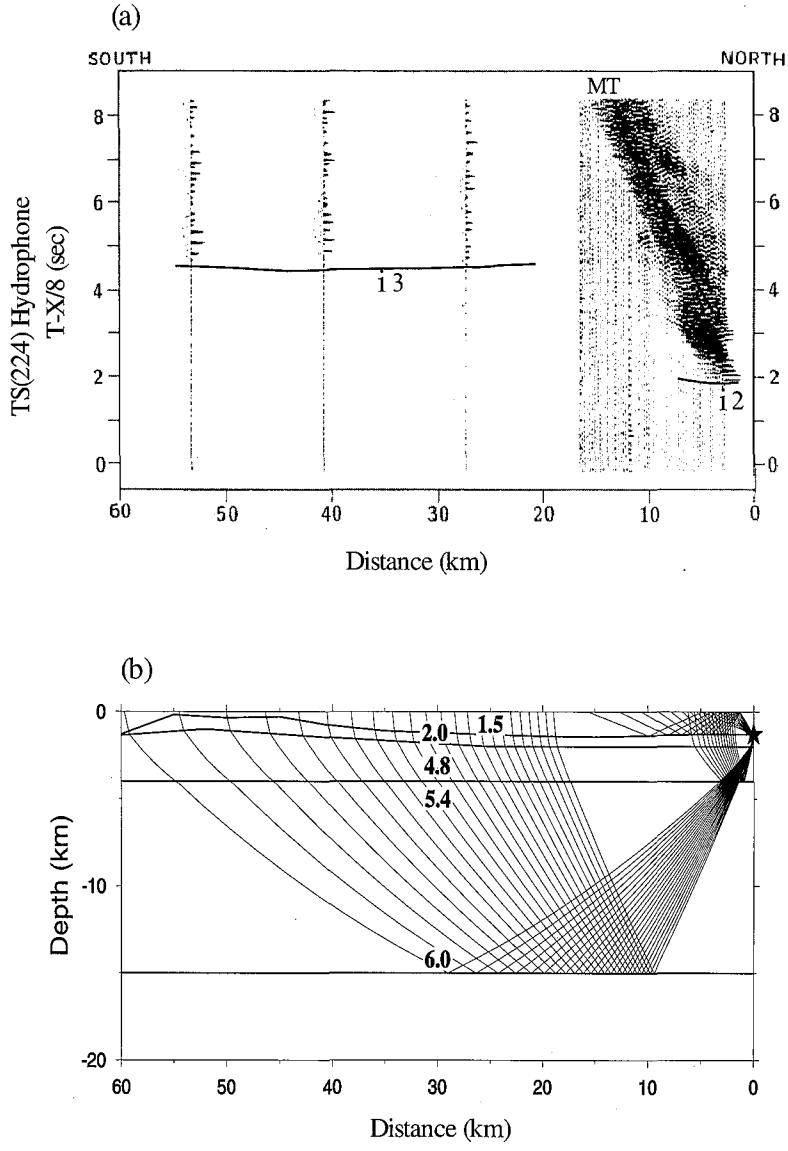

Fig. 10. (a) Observed seismograms and predicted travel time curves of profile L85-2. The phase, i3, in an offset range of 27-54 km is interpreted as reflected waves from a lower intercrustal layer (PiP phase). The MT phases are explained as multiples. (b) Velocity structure and ray diagram, with the vertical exaggeration taken as 1.6:1.

neath. It is also noteworthy that the bottom of the 5.2-5.8 km/s layer increases its depth northward from 24°N. This could be explained as a zone of prominent subhorizontal reflectors which occurs in the midcrust, signifying the upper part of the subducting plate.

The velocity structure of profile L85-1 which crosses the Yaeyama Ridge (Figures 11b and 9), shows a similarity to those in L93-1 through L93-5, which represent the velocity struc-

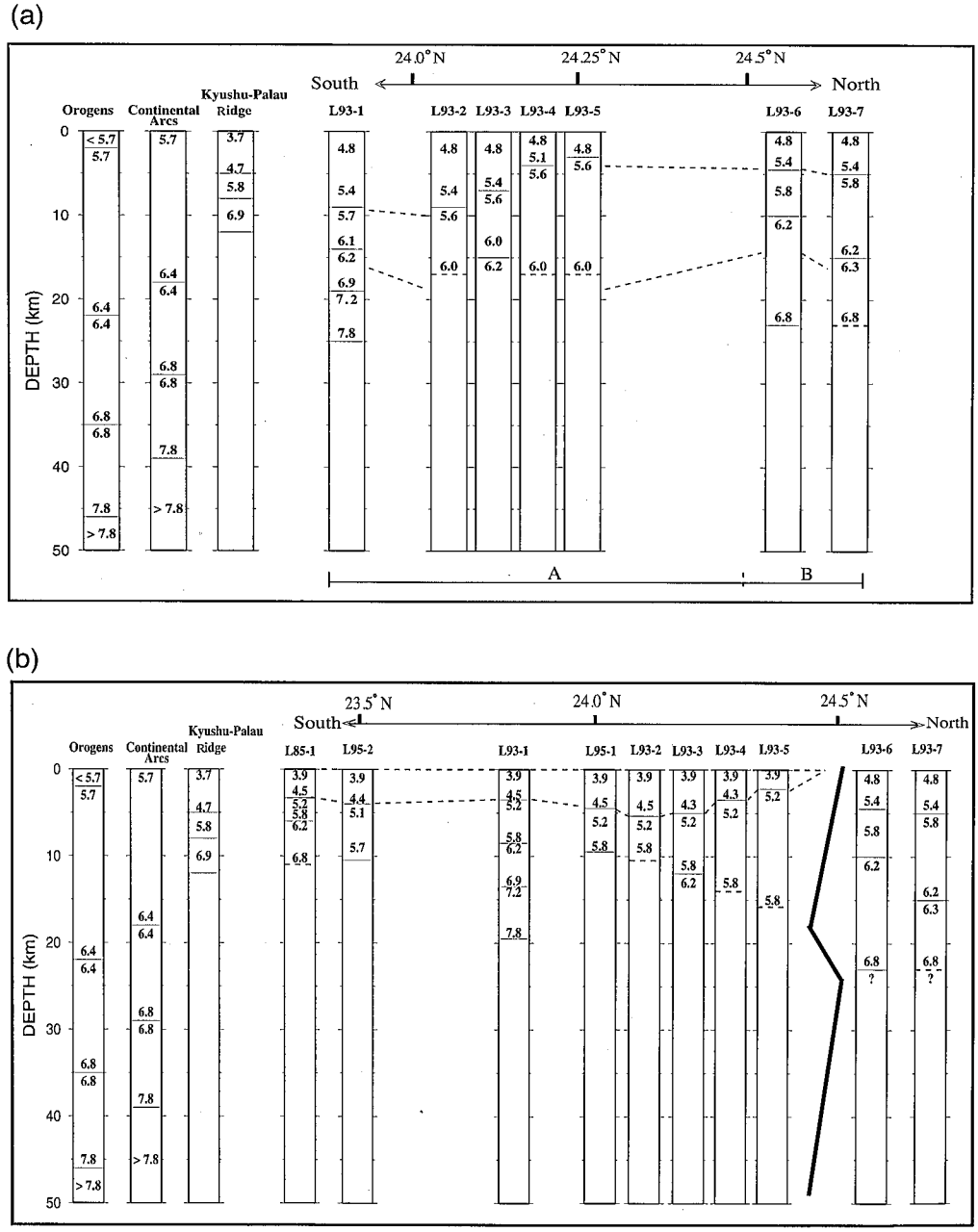

Fig. 11. Comparison between the average crustal velocity structures of orogens, continental arcs and the Kyushu-Palau Ridge (the three on the left) and the velocity models to the west (a) and east (b) of the LV fault constructed in this study (without water and sedimentary layer). The shaded parts show the distribution of the velocity structure ranging from about 5.7 km/s to 6.4 km/s. See text for explanation.

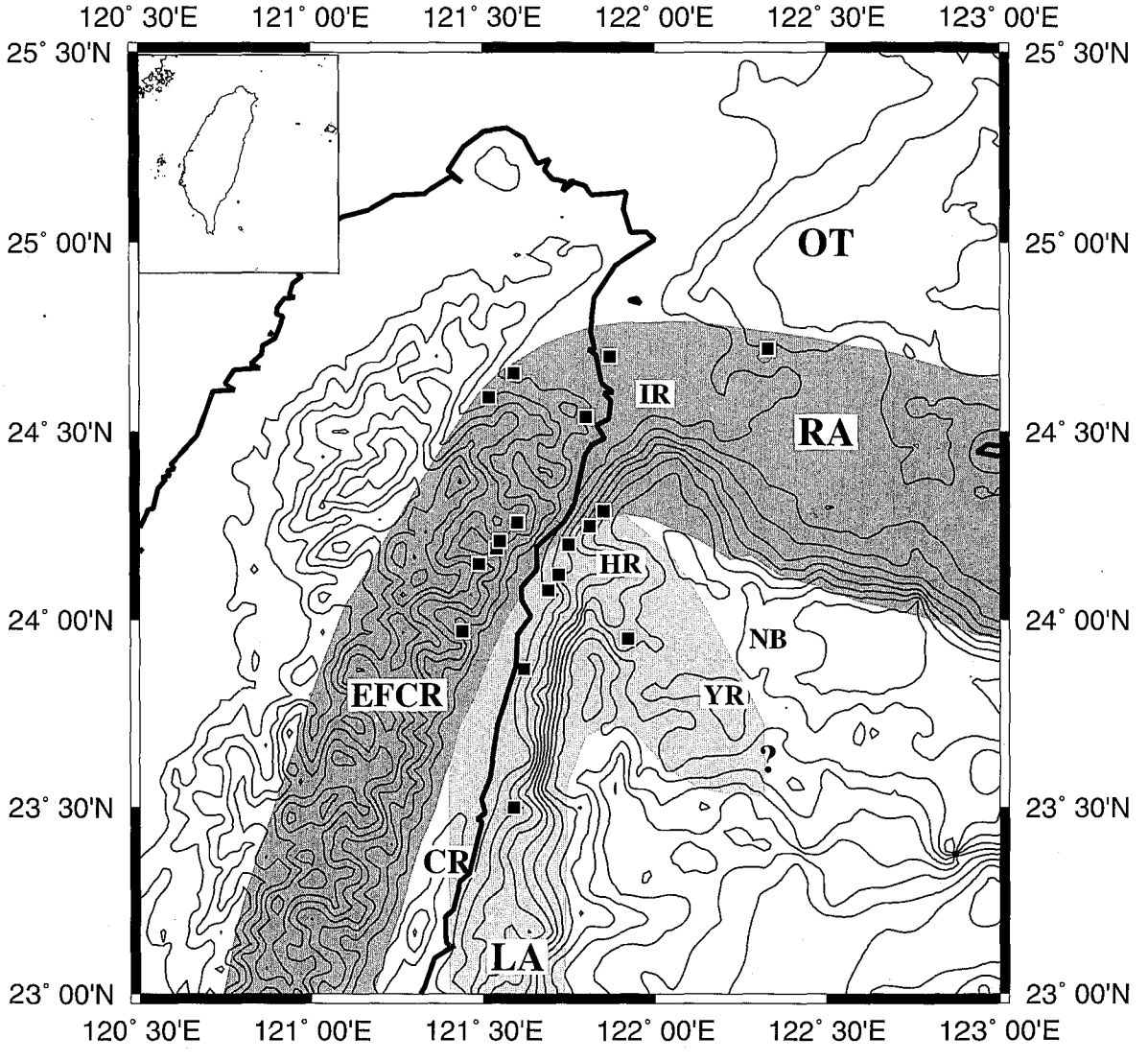

Fig. 12. Scheme of the tectonic provinces (shaded zones) and boundaries based on the results of the modeling in this study. The solid squares indicate the locations of the velocity columns shown in Figure 11. Note the eastern flank of the Central Range (EFCR) has bent and extends eastward at 24.5°N and should belong to the same tectonic unit as the southwestern Ryukyu arc (RA). The velocity structure of the Hsinchen Ridge (HR) and the Yaeyama Ridge (YR) could be the same type of tectonic unit as the Coastal Range (CR). OT represents the Okinawa Trough; NB is the Nanao Basin; and IR is the Ilan Ridge.

tures of the CR. From the seismic reflection study of Lin (1994), the CR, HR and YR all show a region without coherent reflections or obvious layer structure. On the basis of this evidence, it is suggested that the velocity structure of the HR and YR might share the same type of tectonic unit as the CR (Figure 12).

For a long time, it has been believed that the island of Taiwan is the result of an active oblique collision between the Asian continental margin and the overriding Luzon arc of the Philippine Sea plate (e.g., Biq, 1973; Bowin *et al.*, 1978; Suppe, 1984; Letouzey and Kimura, 1986; Ho, 1986). This means the weak sediment layers of the Asian continental margin were deformed and uplifted by the collision of the stronger Luzon arc thereby forming the Taiwan mountain belt.

In direct opposition, when the resultant velocity structures of this study are compared with those from other tectonic units (Figure 11), the velocity structure of the CR which represents the tectonic unit of the Luzon arc seems similar to the Kyushu-Palau Ridge in terms of its velocity features. In addition, the velocity structure of the EFCR is similar to the continental arc. Obviously, the strength of the material of the EFCR should be stronger and heavier than that of the CR. This implies that the CR played a weaker role in its collision with the EFCR. Hence, the resultant velocity structure of this study suggests that the mechanism of the collision between the EFCR and CR exhibits dramatic evidence contradicting the notion of a typical arc-continental margin collision. Beside this, it also suggests that our results are consistent with the arc-arc collision model (Hsu and Sibuet, 1995) in the northeastern Taiwan area.

5. CONCLUSIONS

The main conclusions of this study can be summarized as follows:

(1) The P-wave velocity from the surface to the depth of 12-15 km varies from 3.9 to 5.8 km/s beneath the Coastal Range (CR) and from 4.8 to 6.1 km/s beneath the eastern flank of the Central Range (EFCR). After comparing the resultant velocity models obtained in this study with those of other tectonic units, it is concluded that the CR is an oceanic arc, while the EFCR is a continental arc.

(2) On the basis of the velocity structure, the CR extends northward to 24.2°N, and the Hsinchen Ridge and the Yaeyama Ridge should have the same type of tectonic unit as the CR.

(3) The Ilan Ridge, located at the southwestern end of Ryukyu arc, is the northeastern extension of the EFCR. This suggests that the EFCR probably bends eastwards and belongs to the same tectonic unit as the southwestern Ryukyu arc.

(4) Based on the velocity structure, the CR is lighter and weaker than the EFCR. This contradicts with the arc-continental collision model which suggests that the island of Taiwan is the result of the collision of the stronger Luzon arc against the weaker Asian continental margin.

Acknowledgments The authors grateful to S.-K. Hsu for his helpful discussion during this research. Thanks are also due to the members of the Institute of Earth Sciences, Academia Sinica and the Seismological Observation Center, Central Weather Bureau for their efforts in data collection. The anonymous reviewers have greatly improved the manuscript. Maps were generated by GMT software released by P. Wessel and W. H. F. Smith. This study was supported by the National Science Council of the R.O.C.

REFERENCES

Biq, C. -C., 1965: The east Taiwan rift. *Petrol. Geol. Taiwan*, **4**, 93-106.

Biq, C. -C., 1973: Kinematic pattern of Taiwan as an example of actual continent-arc collision. Report of the Seminar on Seismology, US-ROC Cooperative Science Program, 21-26.

Bowin, C., R. -S. Lu, C. -S. Lee, and H. Schouten, 1978: Plate convergence and accretion in the Taiwan-Luzon region. *Am. Assoc. Petrol. Geol. Bull.*, **62**, 1645-1672.

Cerveny, V., A. Molotkov, and I. Psencil, 1977: Ray Methods in Seismology, University of Karlova Press, Prague, Czechoslovakia. 214pp.

Chen, Q. -B. and C. -Y. Wang, 1994: The seismic experiment in the Longitudinal Valley near Hualien city. Proc. Fifth Taiwan Symposium on Geophysics, 247-251.

Chen, Y. -L., 1995: Three dimensional velocity structure and kinematic analysis in the Taiwan area. Master Thesis, National Central Univ., 172pp (in Chinese).

Cheng, W. -B. and C. Wang, 1995: Study on the mechanism of the generation and propagation of the multiples in water (abstract). Annual meeting of the Geophysical Society of China, p. 20 (in Chinese).

Chiu, J. -M., G. Steiner, R. Smalley, Jr., and A. C. Johnston, 1991: PANDA: a simple, portable seismic array for local- to regional-scale seismic experiments. *Bull. Seis. Soc. Am.*, **81,** 1000-1014.

Christensen, N. I. and W. D. Mooney, 1995: Seismic velocity structure and composition of the continental crust: a global view. *J. Geophys. Res.*, **100**, 9761-9788.

Clossley, D., 1987: RAYAMP-PC: a PC program for 2-D ray-tracing and synthetic seismograms, Version 2.0, Geophysics Laboratory, McGill University.

Hagen, R. A., F. K. Duennebier and V. Hsu, 1988: A seismic refraction study of the crustal structure in the active seismic zone east of Taiwan. *J. Geophys. Res.*, **93**, 4785-4796.

Ho, C. -S., 1986: A synthesis of the geologic evolution of Taiwan. *Tectonophysics*, **125**, 1-16.

Hsu, S. -K., J. C. Sibuet and C. -T. Shyu, 1996: High-resolution detection of geologic boundaries from potential field anomalies: an enhanced analytic signal technique. *Geophysics*, **61**, 373-386.

Hsu, S. -K. and J. C. Sibuet, 1995: Is Taiwan the result of arc-continent or arc-arc collision?. *Earth Planet. Sci. Lett.*, **136**, 315-324.

Hu, C. -C., and W. -S. Chen, 1986: Gravity and magnetic anomalies of eastern Taiwan. Mem. *Geol. Soc. China*, **7**, 341-352.

Kennett, B. L. N., 1977: Towards a more detailed seismic picture of the oceanic crust and mantle. *Mar. Geophys. Res.*, **3**, 7-42.

Kizaki, K., 1986: Geology and tectonics of the Ryukyu islands. *Tectonophysics*, **125**, 193-207.

Lee, C. -W., C. Wang and Z. -S. Liaw, 1986: A study of the crustal velocity structure in eastern Taiwan. *Bull. Inst. Earth Sci., Academia Sinica*, **6**, 95-108.

Lin, S. -C., 1994: Bathymetry and seismic characteristics offshore eastern Taiwan, and its tectonic implications. Master Thesis, National Taiwan Univ. 78pp (in Chinese).

Letouzey, J. and M. Kimura, 1986: The Okinawa Trough: Genesis of a back-arc basin developing along a continental margin. *Tectonophysics*, **125**, 209-230.

Liu, C. -S., 1995: Deep seismic imaging of the Taiwan arc-continent collision zone. Workshop for Integrated Oceanographic Research Programs, December 6-9, Taoyuan, T15-19.

Ludwig, W., S. Murauchi, N. Den, P. Bull, H. Hotta, M. Ewing, T. Asanuma, T. Yoshii and N. Sakajiri, 1973: Structure of the East China Sea-West Philippine Sea margin off southern Kyushu, Japan. *J. Geophys. Res.*, **78**, 2526-2536.

Lundberg, N. and R. J. Dorsey, 1988: Synorogenic sedimentation and subsidence in a Plio-Pleistocene collision basin, eastern Taiwan. In: K. L. Kleinspehn and C. Paolo (Eds.), New Perspective in Basin Analysis. Springer, New York, 265-280.

Ma, K. -F., Wang, J. -H. and D. Zhao, 1996: 3-D seismic structure of the crust and uppermost mantle beneath Taiwan, *J. Phys. Earth.*, **44**, 85-105.

Pelletier, B. and J. F. Stephan, 1986: Middle Miocene obduction and late Miocene beginning of collision registered in the Hengchun peninsula: geodynamic implications for the evolution of Taiwan. *Tectonophysics*, **125**, 133-160.

Song, G. -S., 1994: Bathymetry of offshore northeast of Taiwan, 1: 150000. Chinese Naval Hydrographic and Oceanographic Office, Republic of China.

Suppe, J., 1984: Kinematics of arc-continent collision, flipping of subduction, and back-arc spreading near Taiwan. *Mem. Geol. Soc. China*, **6**, 21-34.

Tsai,Y. -B., Y. -M. Hsiung, H. -B. Liaw, H. -P. Lueng, H. -P. Yao, Y. -H. Yeh and Y. -T. Yeh, 1974: A seismic refraction study of eastern Taiwan. *Petrol. Geol. Taiwan*, **11**, 165-182.

Tsai, Y. -B., Z. -S. Liaw, T. -Q. Lee, M. -T. Lin and Y. -H. Yeh, 1981: Seismological evidence of an active plate boundary in the Taiwan area. *Mem. Geol. Soc. China*, **4**, 143-154.

Yu, S. -B., D. D. Jackson, G. -K. Yu and C. -C. Liu, 1990: Dislocation model for crustal deformation in the Longitudinal Valley area, eastern Taiwan. *Tectonophysics*, **183**, 97-109.

Yu, H. -S. and E. Hong, 1992: Physiographic characteristics of continental margins, northeast Taiwan. *TAO*, **3**, 419-434.

Wang, C., K. -F. Li, H. -H. Huang and C. -F. Huan, 1995: Analysis of the travel times of artificial P-waves in the Hualien area of Eastern Taiwan. *Acta Oceanographica Taiwanica*, **34**, 61-72.

Whitmarsh, R. B., 1978: Seismic refraction studies of the upper igneous crust in the north Atlantic and porosity estimates for layer 2. *Earth Planet. Sci. Lett.*, **37**, 451-464.

Yen, T. -P., 1954: The geneisses of Taiwan. *Bull. Geol. Surv. Taiwan*, **5**, 1-100.